ELSEVIER

Journal of Alloys and Compounds 216 (1994) 213–220

Journal of ALLOYS AND COMPOUNDS

Morphological and structural studies of amorphous $Fe_{74}Cr_{18}Ni_8$ alloy prepared by the rod-milling technique

M. Sherif El-Eskandarany[a], H.A. Ahmed[b]

[a]*Mining and Petroleum Engineering Department, Faculty of Engineering, Al-Azhar University, Nasr City, Cairo, Egypt*
[b]*Mining, Petroleum and Metallurgical Engineering Department, Faculty of Engineering, Cairo University, Giza, Egypt*

Received 8 April 1994

Abstract

The mechanical alloying process has been used for the formation of an amorphous austenitic stainless steel ($Fe_{74}Cr_{18}Ni_8$) alloy by dry milling elemental powders of b.c.c. Fe, b.c.c. Cr and f.c.c. Ni in a rod mill at room temperature. The progress of the solid state amorphization reaction for the $Fe_{74}Cr_{18}Ni_8$ ternary system has been followed as a function of the milling time by means of X-ray diffraction, an optical microscope, scanning and transmission electron microscopes and differential thermal analysis. The results show that a homogeneous amorphous phase of $Fe_{74}Cr_{18}Ni_8$ alloy powder has been formed after 1080 ks of milling. The powder at the final stage of milling is fine in size (almost 1 μm in diameter) and uniform in shape, with a sphere-like morphology. The thermal stability indexed by the crystallization temperature T_x of $Fe_{74}Cr_{18}Ni_8$ amorphous alloy shows that the amorphous austenitic stainless steel is very stable up to temperatures as high as 1240 K. Above this temperature the amorphous phase is transformed to an ordered phase of f.c.c. $Fe_{74}Cr_{18}Ni_8$ (the typical structure of austenitic stainless steel). The enthalpy change of crystallization, ΔH_x, is measured as -16.88 kJ mol^{-1}.

Keywords: Rod-milling technique; Mechanical alloying; Thermal stability

1. Introduction

In 1983 Koch et al. [1] introduced the first application of mechanical alloying (MA) [2] for preparing a single amorphous phase of $Ni_{60}Nb_{40}$ alloy powder by milling elemental metallic powders of Ni and Nb in a ball mill under an inert gas. It is believed that the MA process is based on a solid state amorphization reaction (SSAR) [3] taking place at the interfaces of the layers in the composite powder particles. The MA process through ball-milling and/or rod-milling techniques has been widely used for preparing several amorphous alloys [4–14], especially those that are difficult to obtain by traditional processes [15–18]. It has also been used for preparing nanocrystalline alloys [19,20].

Apart from the amorphization reaction via the mechanical reaction in a ball mill, El-Eskandarany et al. [21] have shown that the ball-milling technique can be successfully used for preparing metal nitride alloys [22–25] by milling the elemental powders under a nitrogen gas flow at room temperature.

Traditionally, steel and steel alloys are prepared by the conventional casting technique. The present work proposes an attractive technique for preparing austenitic stainless steel ($Fe_{74}Cr_{18}Ni_8$) by rod milling elemental powders of Fe, Cr and Ni at room temperature. One significant potential technological attraction of the present study is that it offers an industrial application of the MA process for producing an alloy which has great interest for engineers and material scientists. Moreover, the end-product of amorphous steel powder and/or annealed stainless steel (f.c.c. structure) can be used as a powder for high corrosion resistance coatings or can be consolidated by cold or hot pressing, thereby offering the prospect of manufacturing bulk metallic alloys made from amorphous (below the crystallization temperature) and/or crystalline (above the crystallization temperature) steel phases by a simple and powerful technique.

Finally, the present work has been addressed in part to studying the morphology, structure and thermal stability behaviours of amorphous $Fe_{74}Cr_{18}Ni_8$ alloy powder.

0925-8388/95/$09.50 © 1995 Elsevier Science S.A. All rights reserved
SSDI 0925-8388(94)01282-M

2. Experimental details

2.1. Materials

High purity (99.99%) elemental metallic powders of Fe (75 μm), Cr (50 μm) and Ni (100 μm) have been used as starting materials.

2.2. Type of mill

The rod mill used in this study has been designed so that its length (250 mm) is greater than its diameter (120 mm) and the rods (SUS 304, 10 mm in diameter) have been cut to lengths (200 mm) less than the full length of the shell. The movement of the rods (10 rods) inside the shell was directly observed through a thick and transparent plastic plate sealing the window of the shell. This observation has shown that the milling process occurs by the line contact of rod–powder–rod extending over the full length of the shell. More details of this mill can be found in a previous paper [10]. The rod-milling process was carried out by mounting the shell on a rotator running at a rate of 1.4 s^{-1}.

2.3. Sample preparation

The starting materials of the MA process were placed in a glove-bag filled with Ar gas (O_2 and H_2O were less than 10 ppm) together with the milling tools. The elemental powders of Fe, Cr and Ni metals were balanced and blended in the glove-bag using an agate mortar and pestle to give the desired composition of the $Fe_{74}Cr_{18}Ni_8$ ternary system. The blended powders were sealed in the mill together with the milling media. The milling process was stopped at regular intervals and a small amount of the milled powder was removed from the vial for various analyses.

2.4. Analyses

2.4.1. X-Ray diffraction

Powder X-ray diffraction (XRD) data were obtained with a Philips–Norelco diffractometer operating in the θ–2θ scan mode with Cu Kα radiation at 35 kV and 20 mA. The sample was attached to double-sided sticky transparent tape mounted on a microscope slide and placed in the area irradiated by X-rays.

2.4.2. Thermal analyses

The crystallization behaviour of amorphous $Fe_{74}Cr_{18}Ni_8$ alloy has been monitored by differential thermal analysis (DTA) at a heating rate of 0.67 K s^{-1} in purified argon gas. In all DTA measurements the samples were heated to 1300 K and cooled to about 500 K, then reheated in second heating run to find the baseline. X-Ray diffraction was used to confirm the exothermic peak.

2.4.3. Metallography

The metallography of the alloyed powder has been studied using a scanning electron microscope (SEM) equipped with an electron probe microanalyser (EPMA) operated at 20 kV and a light optical microscope. In these experiments a small amount of the alloyed powder was placed in a plastic holder (epoxy) and wet ground carefully using fine silicon carbide emery papers (800–1500 mesh). The grinding process was performed using paraffin as a lubricant to prevent particles of emery being embedded in the surface of the specimen. Then the sample was polished on lapping tape (2000–6000 mesh) wetted by kerosene. Finally the specimen was polished on silk cloth using a solution of white wax in benzene. Care was taken to obtain a satisfactory surface without any distortions. Then the specimen was etched using HCl (0.1 N) activated with five drops of H_2O_2 (10%).

2.4.4. Morphology

The morphology of the alloyed powder was examined using a 20 kV SEM and a 200 kV transmission electron microscope (TEM). For the SEM observations a small amount of the powder was put on a copper holder coated with carbon dutite. The samples for TEM observations were prepared by crushing the powder under ethanol to make a suspension and dropped on a microgrid made of copper, then dried for 3 hours in a drying furnace at about 390 K.

2.4.5. Chemical analyses

The chemical analyses were performed using an ICP interfaced to a microcomputer in order to detect exactly the contents of Fe, Cr and Ni. For these analyses an amount of the milled powder (about 30 mg) was dissolved in a leaching solution (HF (1 N), 2 ml; H_2SO_4 (6 N), 10 ml; HNO_3 (6 N), 40 ml; H_2O_2 (36 wt.%), 2 ml) in a platinum container (100 ml in volume). Then the solution was heated slowly until the powder dissolved completely without any precipitation. The solution was diluted with pure water in a volumetric mass flask (100 ml in volume). The ICP was calibrated by Fe, Cr and Ni standard solutions before analysing the sample. Each component for each sample was analysed five times for more accuracy.

3. Results

3.1. Structural change with the milling time

X-Ray analyses were performed in order to understand the total structure of $Fe_{74}Cr_{18}Ni_8$ alloy powder

at various stages of the rod-milling process. Fig. 1 displays the XRD patterns of $Fe_{74}Cr_{18}Ni_8$ alloy powder after selected MA times. After 2 ks of MA (initial stage) the mill discharge consists of b.c.c. Fe, b.c.c. Cr and f.c.c. Ni in elemental form. The Bragg peaks of pure Fe, Cr and Ni decrease in intensity and become broad at the end of the initial stage of MA (86 ks). After 173 ks of MA all the Bragg peaks of b.c.c. Cr and f.c.c. Ni crystals have completely disappeared. In addition, the Bragg peaks of b.c.c. Fe crystal have become broader and their positions have shifted markedly to the low angle side, indicating the formation of b.c.c. FeCrNi solid solution. It is worth noting that after 360 ks of MA (intermediate stage) these peaks become broader with diffuse haloes, suggesting the formation of an amorphous phase coexisting with b.c.c. FeCrNi solid solution (Fig. 1). At the final stage of MA (1080 ks) the b.c.c. FeCrNi solid solution phase has been completely transformed to a homogeneous amorphous phase characterized by diffuse haloes and smooth peaks. We should emphasize that this amorphous phase has not been changed to any other phase(s) even for samples milled for times as long as 1800 ks (Fig. 1).

The lattice constant a_0 of rod-milled $Fe_{74}Cr_{18}Ni_8$ alloy powder estimated from XRD measurements is shown in Fig. 2 as a function of the MA time. Obviously the b.c.c. FeCrNi solid solution expands with increasing MA time, as characterized by a monotonic increase in a_0 to a value of 0.2878 nm after 360 ks of MA. We should emphasize that this value is larger than that of pure Fe crystal (0.28664 nm), suggesting an interstitial solubility of Cr and Ni in Fe.

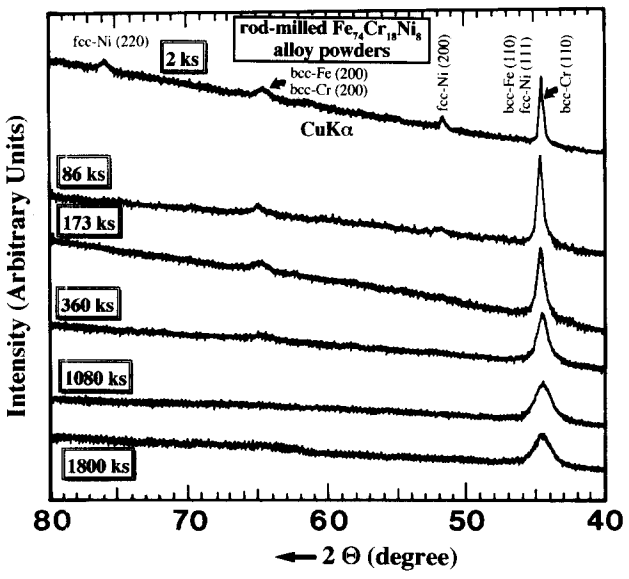

Fig. 1. Effect of MA time on structure of rod-milled $Fe_{74}Cr_{18}Ni_8$ alloy powder.

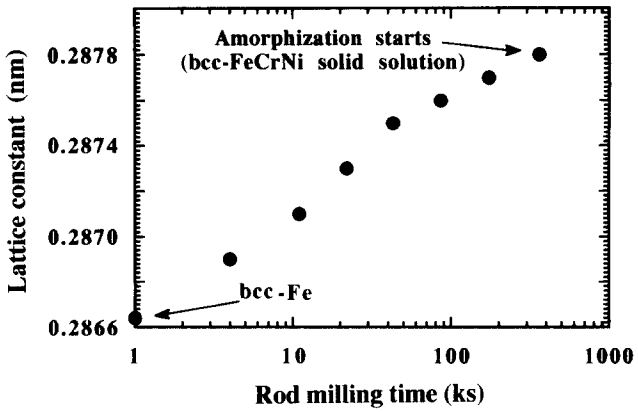

Fig. 2. Effect of MA time on lattice constant a_0 of b.c.c. Fe during rod milling of elemental b.c.c. Fe, b.c.c. Cr and f.c.c. Ni powders.

3.2. Morphology and metallography changes with the milling time

The SEM technique was used to follow the change in morphology of mechanically alloyed $Fe_{74}Cr_{18}Ni_8$ alloy powder at various MA times. Detailed SEM observations after several stages of the MA process are presented in Fig. 3. At the initial stage of milling (2 ks), the powder particles that contain a mixture of elemental Fe, Cr and Ni have a random size with a block-like morphology (Fig. 3a). After a few kiloseconds of MA (22 ks) the starting elemental powders have agglomerated to form composite particles about 600 μm in diameter with a plate-like morphology (Fig. 3b). At this stage of milling, the powder particles have a thick layered structure morphology with a random distribution (Fig. 4a). Increasing the MA time (43 ks) enhances the shear and impact forces generated by the rods, leading to the formation of composite powder particles containing thin or narrow layers of the elemental powders in a regular arrangement and each individual layer has a width of about 10 μm or less (Fig. 4b).

During the progress of the MA process (173 ks) the assemblage of particles has continuously disintegrated to form powder particles that are almost regular in shape (sphere-like morphology) and size (10–20 μm) (Fig. 3c). Metallographic examination of the cross-section of polished and etched particles after this stage of milling shows that the layered structure morphology has already disappeared and the individual particles have no detail on their polished surfaces (Fig. 4d). At the end of the MA process (1080 ks) the powder particles are fairly uniform in size (0.5–1 μm in diameter) (Fig. 3d).

Figs. 5 and 6 summarize the SEM observations of mechanically alloyed $Fe_{74}Cr_{18}Ni_8$ alloy powder at various stages of milling. Obviously the mechanical reaction performed by the MA process can be classified into three stages, i.e. initial, intermediate and final stages. In the early stage the elemental powders of Fe, Cr

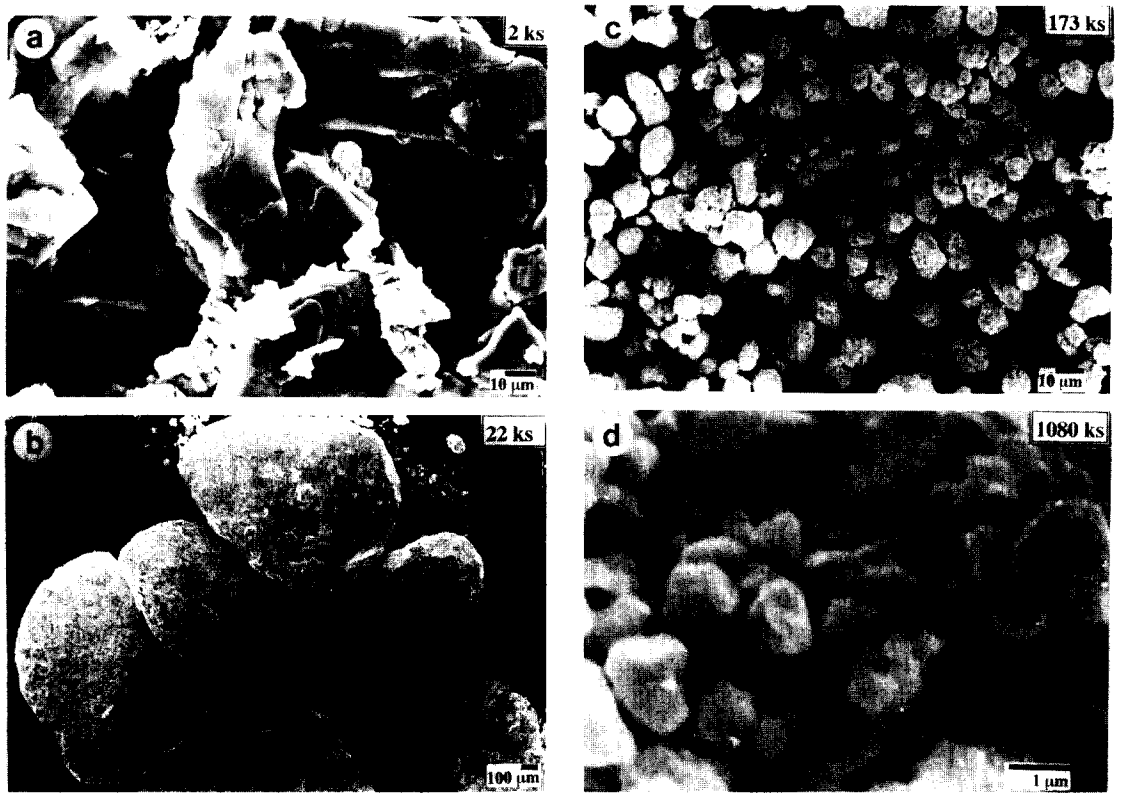

Fig. 3. SEM images of rod-milled $Fe_{74}Cr_{18}Ni_8$ alloy powder particles after various MA times.

and Ni have agglomerated and grown in size as a result of the repeated cold welding. During this stage of milling, the powders vary widely in size from 50 to 800 μm (Fig. 5) and the thickness of the layers in the formed composite powder particles increases dramatically and is widely distributed (Fig. 6). At the subsequent intermediate stage (second stage of milling) the agglomerated powder particles are subjected to a continuous disintegration with fragmentation to form finer powders less than 100 μm in diameter. Furthermore, this stage of milling provides powder particles with a narrow size distribution (Fig. 5). In parallel, the thickness of the metallic layers decreases at this stage, becoming uniform with a narrow thickness distribution (Fig. 6). Towards the end of the MA process (the final stage) all the powder particles are uniform and homogeneous in size (Fig. 5) without any structural detail (Fig. 6).

Detailed TEM analyses were performed in order to observe the structural change of rod-milled $Fe_{74}Cr_{18}Ni_8$ powder during the above-mentioned stages of milling. Bright field images (BFIs) and/or dark field images (DFIs) together with selected area diffraction patterns (SADPs) of mechanically alloyed $Fe_{74}Cr_{18}Ni_8$ powder after selected MA times are shown Fig. 7. Fig. 7a shows the BFI and corresponding SADP after 22 ks of MA. The powder is a mixture of polycrystalline Fe, Cr and Ni with grain boundary fringes and dislocations in the boundary. The SADP taken at the centre of the micrograph reveals a sharp spot pattern related to b.c.c. Fe coexisting with b.c.c. Cr and f.c.c. Al crystals (inset of Fig. 7a). The DFI has been used in order to determine the crystalline size of the alloy powder in a direct way. Fig. 7b shows the DFI and corresponding SADP of $Fe_{74}Cr_{18}Ni_8$ alloy powder after 86 ks of MA. The powder particles have a cell-like morphology containing very fine grains with nanodimensions (about 50 nm or less in diameter). The Debye–Scherrer rings of the SADP reveal the formation of b.c.c. FeCrNi solid solution coexisting with unprocessed Cr and/or Ni (fine spots) (inset of Fig. 7b). Increasing the MA time leads to longer impact and shear forces generated by the rods and this causes mechanical defects in the powder particles. Numerous faults and dislocations appear clearly in the particles after 22 ks of milling (Fig. 7b). Moreover, several defects with grain boundary movement are clearly seen near the centre of the micrograph. Fig. 7c shows a high magnification BFI of $Fe_{74}Cr_{18}Ni_8$ alloy powder after 360 ks of MA. The structure of the alloy powder at this stage of milling is fine and a clear halo pattern is observed in the corresponding SADP, suggesting the existence of an amorphous phase (featureless image). This amorphous phase coexisting with b.c.c. FeCrNi solid solution is indicated by the fringe images and spot diffraction pattern seen in Fig. 7c. At the end of the MA process the structure of the overall

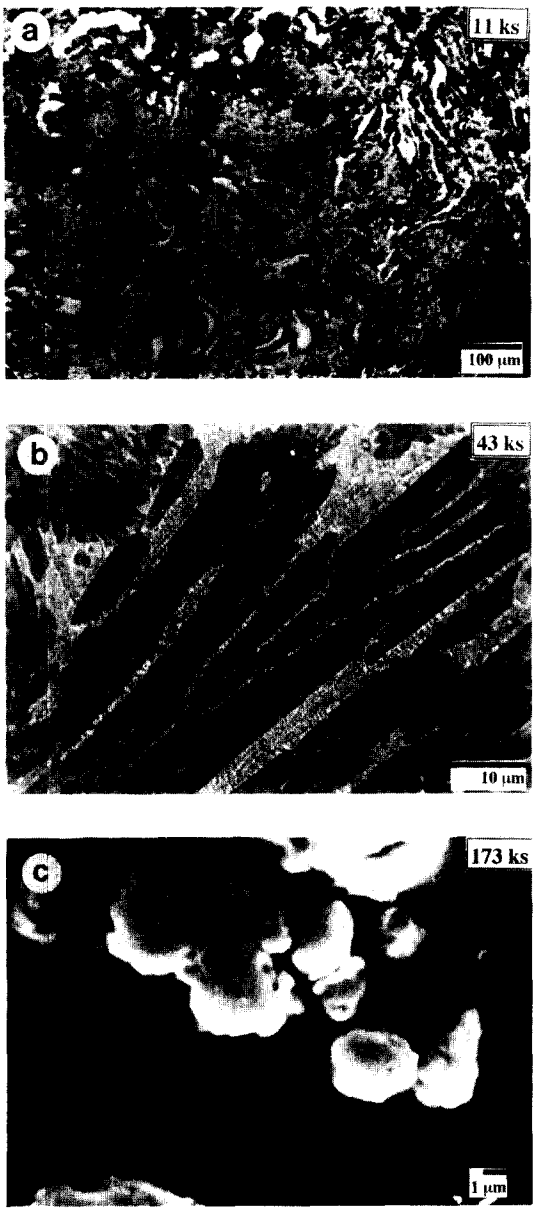

Fig. 4. Cross-sectional views of rod-milled $Fe_{74}Cr_{18}Ni_8$ alloy powder particles after various MA times.

matrix is fine with no dominant facet structure, indicating the formation of an amorphous phase (Fig. 7d). Moreover, the SADP shows a typical halo pattern of an amorphous phase in good agreement with the XRD pattern of Fig. 1.

The TEM technique allows us to determine the crystalline size of $Fe_{74}Cr_{18}Ni_8$ alloy powder during the MA process. These results are in fair agreement with the results of XRD using the Scherrer equation [26], as shown in Fig. 8. The grain size of $Fe_{74}Cr_{18}Ni_8$ alloy powder decreases monotonically with increasing MA time to become almost invisible after 360 ks, i.e. the amorphous starting stage.

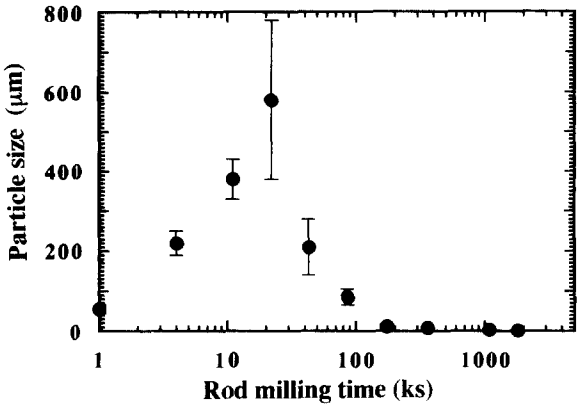

Fig. 5. Particle size distribution of rod-milled $Fe_{74}Cr_{18}Ni_8$ alloy powder as a function of MA time.

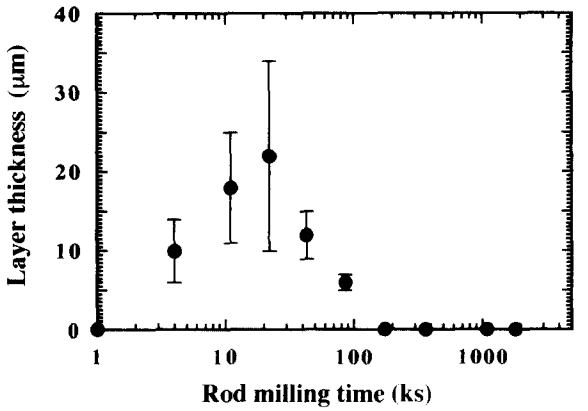

Fig. 6. Effect of MA time on layer thickness of rod-milled $Fe_{74}Cr_{18}Ni_8$ alloy powder particles.

3.3. Thermal analysis

The thermal stability of amorphous $Fe_{74}Cr_{18}Ni_8$ alloy powder has been characterized by DTA measurements. Fig. 9 displays typical DTA curves for amorphous $Fe_{74}Cr_{18}Ni_8$ alloy powder after 1800 ks of MA. During the first heating run (solid curve) a single exothermic peak appears at about 1240 K. In the second heating run (broken curve), however, this exothermic reaction disappeared. In order to understand the origin of this exothermic reaction, the heated sample after the DTA measurements was analysed by XRD. The XRD pattern of this sample shows the formation of f.c.c. $Fe_{74}Cr_{18}Ni_8$ alloy powder (Fig. 10a) in good agreement with the XRD pattern of a standard bulk specimen of austenitic stainless steel (Fig. 10b). Moreover, the BFI of this sample shows the formation of large polycrystalline grains with sharp grain boundaries (Fig. 11). The XRD patterns lead us to attribute the exothermic reaction to an amorphous–crystalline phase transformation at the crystallization temperature T_x of 1240 K with an enthalpy change of crystallization (the area under the exothermic reaction), ΔH_x, of 16.88 kJ mol^{-1}.

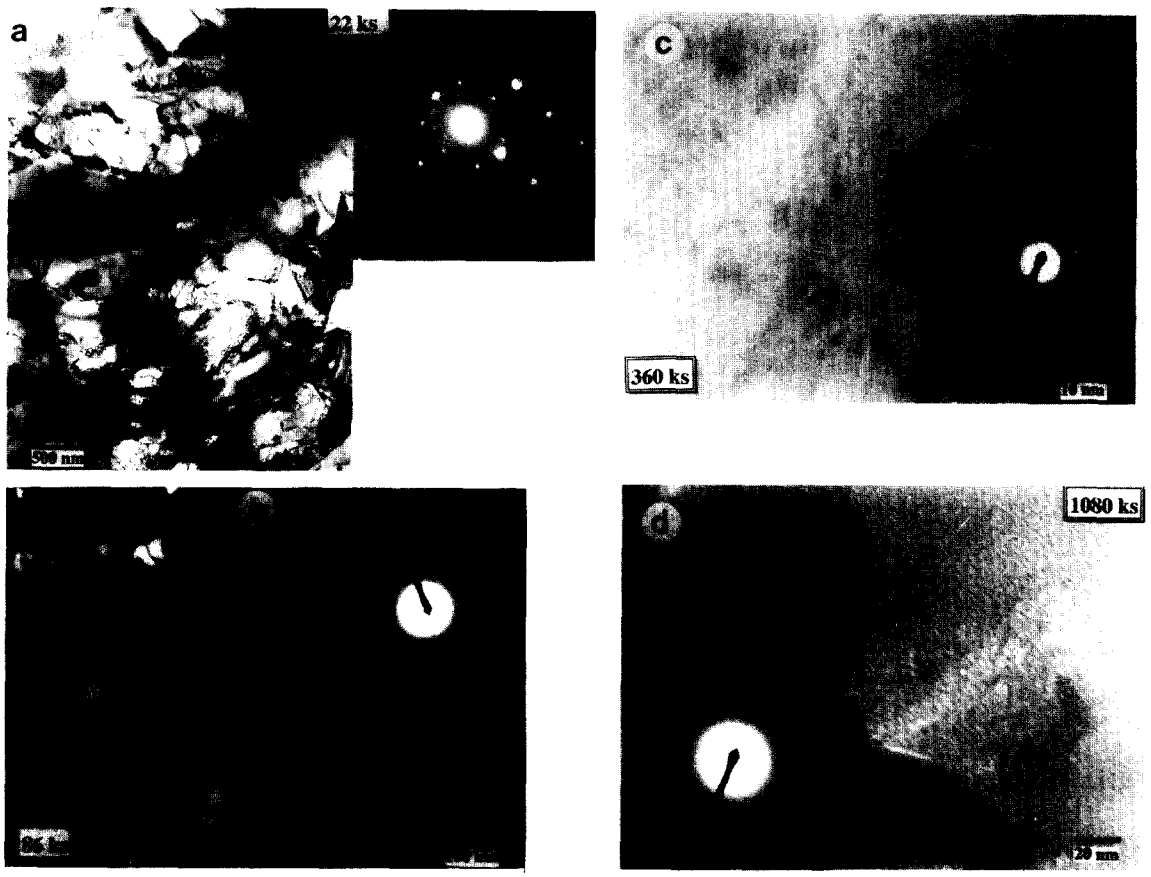

Fig. 7. TEM images and corresponding electron diffraction patterns of rod-milled $Fe_{74}Cr_{18}Ni_8$ alloy powder after various MA times.

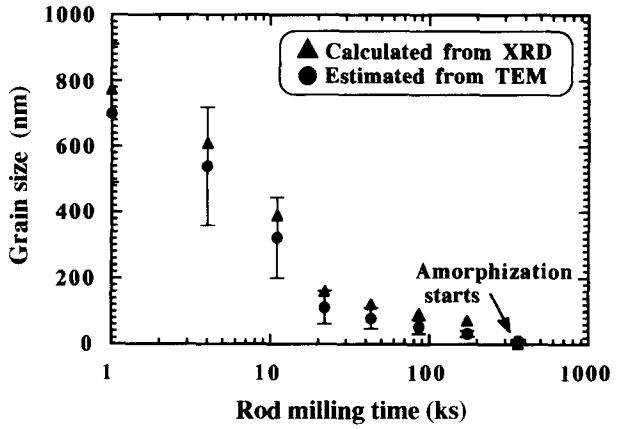

Fig. 8. Effect of MA time on grain size of rod-milled $Fe_{74}Cr_{18}Ni_8$ alloy powder.

4. Discussion

Mechanical alloying of mixed elemental Fe, Cr and Ni powders under an argon gas atmosphere leads to the formation of amorphous $Fe_{74}Cr_{18}Ni_8$ alloy powder. The results have shown that the so-called MA process for producing amorphous $Fe_{74}Cr_{18}Ni_8$ alloy powder can be classified into three main stages. The end-product of each stage varies widely in terms of structure, morphology and metallography. In this section we shall discuss the mechanism of amorphization of austenitic stainless steel via the MA process through each stage of milling.

4.1. The early stage

During the first few kiloseconds of the MA process, e.g. 2 ks, the powder particles of Fe, Cr and Ni blend together without forming any composite particles (Figs. 1, 3 and 7a). As a result of cold welding, almost all the starting material powders consist of assemblages or agglomerations of Fe, Cr and Ni forming composite particles of larger diameter (Fig. 3b). This stage of milling can also be called the "negative milling stage", in which the size of the powder particles increases. The particles at this stage of the MA process have a well-developed lamellar structure of elemental Fe, Cr and Ni (Fig. 4a).

4.2. The intermediate stage

The previous negative stage of milling is followed by a second stage which is called the intermediate stage or positive stage of milling (22–360 ks). Here the agglomerated particles are shattered and disintegrated

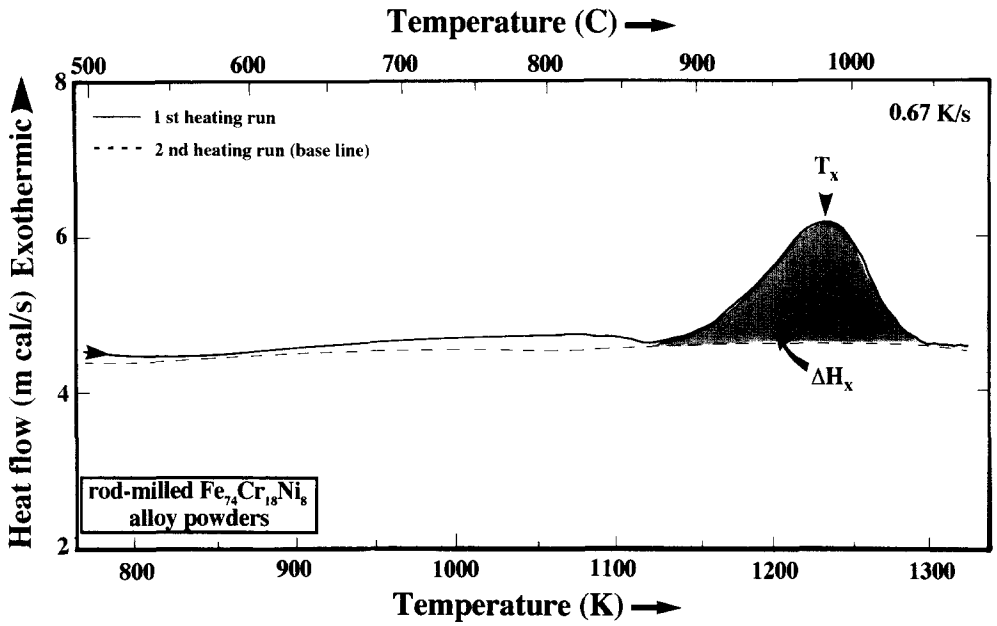

Fig. 9. DTA curve of rod-milled $Fe_{74}Cr_{18}Ni_8$ alloy powder after 1800 ks of MA.

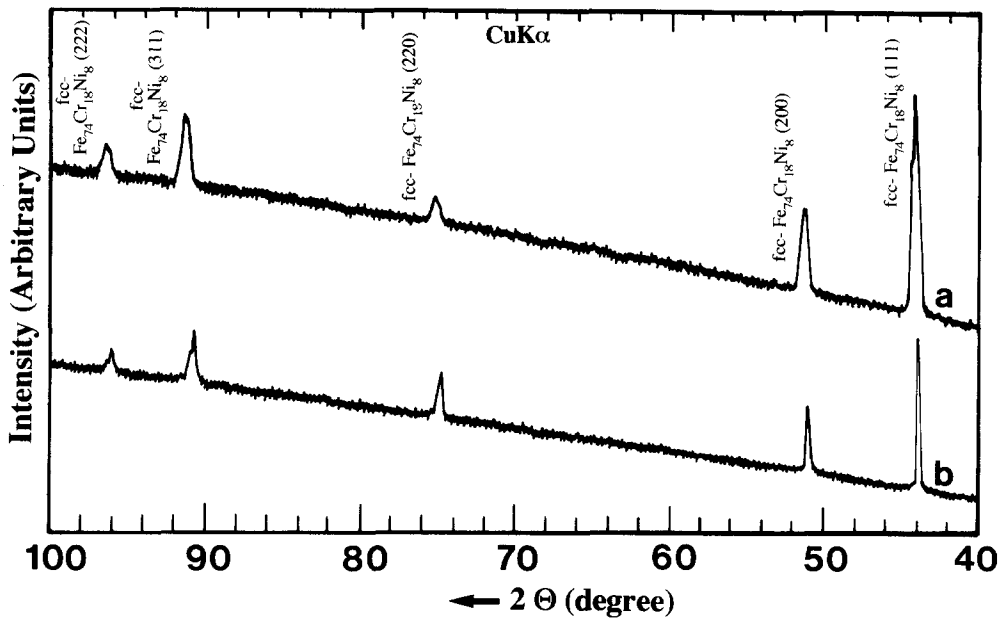

Fig. 10. XRD patterns of (a) $Fe_{74}Cr_{18}Ni_8$ alloy powder milled for 1800 ks, then heated to 1300 K during DTA measurements and (b) standard sample of austenitic stainless steel.

into several particles apparently irregular in shape and size (Fig. 3c). This disintegration of the powder particles has occurred as a result of the continuous shear stress and impact force generated by the rod–powder–rod collisions. As the powders are subjected to these external forces, new or fresh active surfaces of the particles appear. During this stage of the MA process all Bragg peaks of b.c.c. Cr and f.c.c. Ni crystals diffuse completely into the Bragg peaks of b.c.c. Fe crystal, indicating the formation of b.c.c. FeCrNi solid solution (Fig. 1). It is worth noting that the layered structure morphology (Fig. 4b) seen in the cross-sectional view of the particles had already disappeared, suggesting the formation of a single phase (b.c.c. FeCrNi solid solution) (Fig. 4c). As the milling time increases to 360 ks, the b.c.c. solid solution expands to $a_0 = 0.2878$ nm. In fact, this value is larger than that of pure b.c.c. Fe crystal (0.2866 nm), suggesting an interstitial solubility of Cr and Ni in Fe as was illustrated in Fig. 2. Further milling leads to mechanical defects of the powders which give rise to several defects in the FeCrNi solid solution. These defects are able to change the free energy of the solid solution to the less stable phase of amorphous FeCrNi.

Fig. 11. (a) BFI and (b) corresponding SADP of $Fe_{74}Cr_{18}Ni_8$ alloy powder milled for 1800 ks, then heated to 1300 K during DTA measurements.

4.3. The final stage

In the present study we shall define the final stage of the MA process (360–1800 ks) as the homogenization stage in which the solid state reaction takes place homogeneously and a uniform amorphous phase of $Fe_{74}Cr_{18}Ni_8$ alloy is obtained. Towards the end of this stage the amorphous phase has XRD patterns with broad and smooth peaks (Fig. 1). In addition, the amorphous alloy powder crystallizes through a single exothermic peak (Fig. 9), suggesting that the formed amorphous phase is single phase and homogeneous in composition. This amorphous phase is stable at high temperature and transforms to f.c.c. austenitic stainless steel at 1300 K (Fig. 10).

5. Conclusions

The formation of amorphous austenitic stainless steel ($Fe_{74}Cr_{18}Ni_8$) powder at room temperature using the mechanical alloying technique is reported. The amorphous alloy powder has been fabricated by milling elemental Fe, Cr and Ni powders in a rod mill under purified argon gas. The results have shown that the mode of amorphization of the $Fe_{74}Cr_{18}Ni_8$ ternary system via the rod-milling technique can be classified into three stages of milling as follows.

(1) During the first stage the elemental powders of Fe, Cr and Ni particles form layered composite particles of larger diameter as a result of cold welding.

(2) During the second stage the elemental Cr and Ni powders completely diffuse into the Fe matrix to form a b.c.c. FeCrNi solid solution. This solid solution expands with increasing milling time and leads to a saturation value of the lattice parameter a_0 of 0.2878 nm after 360 ks of milling.

(3) During the final stage of milling, further mechanical defects that result from increasing the MA time lead to a transformation of the b.c.c. FeCrNi solid solution into the less stable phase of amorphous $Fe_{74}Cr_{18}Ni_8$ alloy powder. The crystallization characteristics represented by the crystallization temperature T_x and the enthalpy change of crystallization, ΔH_x, are 1240 K and -16.88 kJ mol^{-1} respectively.

One goal of the present study is to offer a powerful and easy technique for the formation of stainless steel alloy at room temperature.

References

[1] C.C. Koch, O.B. Cavin, C.G. McKamey and J.O. Scarbrough, *Appl. Phys. Lett., 43* (1983) 1017.
[2] J.S. Benjamin, *Metall. Trans. A, 1* (1970) 2943.
[3] R.B. Schwarz and W.L. Johnson, *Phys. Rev. Lett., 51* (1983) 415.
[4] K. Suzuki, *J. Non-Cryst. Solids, 117–118* (1990) 1.
[5] M. Sherif El-Eskandarany, K. Aoki and K. Suzuki, *Metall. Trans. A, 23* (1992) 1231.
[6] M. Sherif El-Eskandarany, K. Aoki and K. Suzuki, *J. Appl. Phys., 71* (1992) 2924.
[7] M. Sherif El-Eskandarany, K. Aoki and K. Suzuki, *J. Appl. Phys., 72* (1992) 2665.
[8] M. Sherif El-Eskandarany, K. Aoki, H. Itoh and K. Suzuki, *J. Less-Common Met., 169* (1991) 235.
[9] M. Sherif El-Eskandarany, K. Aoki, T. Masumoto and K. Suzuki, *J. Alloys Comp., 209* (1994) 71.
[10] M. Sherif El-Eskandarany, K. Aoki and K. Suzuki, *J. Less-Common Met., 167* (1990) 113.
[11] M. Sherif El-Eskandarany, K. Aoki and K. Suzuki, *Mater. Sci. Forum, 88–90* (1992) 81.
[12] M. Sherif El-Eskandarany, K. Aoki and K. Suzuki, *J. Non-Cryst. Solids, 150* (1992) 472.
[13] M. Sherif El-Eskandarany, K. Aoki and K. Suzuki, *J. Alloys Comp., 186* (1992) 15.
[14] M. Sherif El-Eskandarany, K. Aoki and K. Suzuki, *J. Alloys Comp., 177* (1991) 229.
[15] M. Sherif El-Eskandarany, F. Itoh, K. Aoki and K. Suzuki, *J. Non-Cryst. Solids, 117–118* (1990) 729.
[16] T. Fukunaga, K. Nakamura, K. Suzuki and U. Mizutani, *J. Non-Cryst. Solids, 117–118* (1990) 700.
[17] E. Gaffet and M. Harmelin, *J. Less-Common Met., 157* (1990) 201.
[18] M. Sherif El-Eskandarany, K. Aoki and K. Suzuki, *Scr. Metall., 25* (1991) 1695.
[19] T. Tanaka, K.N. Ishihara and P.H. Shingu, *Metall. Trans. A, 23* (1992) 2421.
[20] M.J. Tracy and J.R. Groza, *Nano Struct. Mater., 1* (1992) 369.
[21] M. Sherif El-Eskandarany, K. Sumiyama, K. Aoki and K. Suzuki, *Mater. Sci. Forum, 88–90* (1992) 801.
[22] M. Sherif El-Eskandarany, K. Sumiyama, K. Aoki and K. Suzuki, *J. Mater. Res., 7* (1992) 888.
[23] M. Sherif El-Eskandarany, K. Aoki and K. Suzuki, *Appl. Phys. Lett., 60* (1992) 1562.
[24] M. Sherif El-Eskandarany, K. Sumiyama, K. Aoki, T. Masumoto and K. Suzuki, *J. Mater. Res., 9* (1994) 11.
[25] M. Sherif El-Eskandarany, *J. Alloys Comp., 203* (1993) 281.
[26] A. Guinier, *X-Ray Diffraction*, Freeman, San Francisco, CA, 1963, p. 124.